Geological Magazine

www.cambridge.org/geo

Chinese stalagmite $\delta^{18}O$ records reveal the diverse moisture trajectories during the middle to late last glacial period

Huihui Yang[1,2], Yu-Min Chou[2], Xiuyang Jiang[3], Wei Zheng[2], Yaoqi He[4], Yogaraj Banerjee[5,6], Chuan-Chou Shen[5,6], Tsai-Luen Yu[7], Yi Zhong[2], Fabien Humbert[2,8] and Qingsong Liu[2]

[1]School of Environment, Harbin Institute of Technology, Harbin, 150006, China; [2]Center for Marine Magnetism (CM[2]), Department of Ocean Science and Engineering, Southern University of Science and Technology, Shenzhen, 518055, China; [3]Key Laboratory of Humid Subtropical Eco-Geographical Processes, College of Geography Science, Fujian Normal University, Fuzhou, 350117, China; [4]College of Tourism and Air Service, Guizhou Minzu University, Guiyang, 550025, China; [5]High-Precision Mass Spectrometry and Environment Change Laboratory (HISPEC), Department of Geosciences, National Taiwan University, Taipei, 10617, Taiwan ROC; [6]Marine Industry and Engineering Research Center, National Academy of Marine Research, Taipei, 10617, Taiwan ROC; [7]Research Center for Future Earth, National Taiwan University, Taipei 10617, Taiwan ROC and [8]University of Rennes, CNRS, Géosciences Rennes, UMR 6118, Rennes, France

Original Article

Cite this article: Yang H, Chou Y-M, Jiang X, Zheng W, He Y, Banerjee Y, Shen C-C, Yu T-L, Zhong Y, Humbert F, and Liu Q. Chinese stalagmite $\delta^{18}O$ records reveal the diverse moisture trajectories during the middle to late last glacial period. *Geological Magazine* **161**(e7): 1–13. https://doi.org/10.1017/S0016756824000013

Received: 30 June 2023
Revised: 4 December 2023
Accepted: 3 January 2024

Keywords:
stalagmite $\delta^{18}O$; Heinrich stadials; moisture trajectory; East Asian Summer Monsoon; Indian Summer Monsoon

Corresponding authors:
Yu-Min Chou; Email: chouym@sustech.edu.cn;
Xiuyang Jiang; Email: xyjiang@fjnu.edu.cn

Abstract

Based on 30 high-resolution U-Th dating controls, we reconstruct stalagmite $\delta^{18}O$ records from 45 to 15 thousand years ago (ka B.P., before AD 1950) from the Shizhu Cave, which is located in southwestern China under the influence of both the Indian Summer Monsoon (ISM) and the East Asian Summer Monsoon (EASM). By integrating with the other stalagmite $\delta^{18}O$ records in Asia during the middle to late last glacial, our results reveal two main moisture trajectories: one from the Indian Ocean, through the Shizhu Cave towards central China, and the other from the Pacific Ocean to central and northern China. The systematic decrease of the average values of stalagmite $\delta^{18}O$ records from oceans to inland China reveals a spatial pattern of water vapour fractionation and moisture trajectory during the middle to late last glacial. In contrast, the variation amplitude, which is defined as the departures apart from the background $\delta^{18}O$ records during Heinrich stadials 1 to 4 (HS1–HS4), show an increasing trend from the coastal oceans to mid-latitude inland China, presenting a 'coastal-inland' pattern, which can be interpreted by the enhanced East Asian Winter Monsoon (EAWM) and the weakened EASM. More specifically, the enriched stalagmite $\delta^{18}O$ records in the EASM region during HS1 to HS4 are caused by the decreased summer rainfall amount or/and the increased proportion of summer moisture resources from the Pacific Ocean. These new observations deepen our understanding of the complicated stalagmite $\delta^{18}O$ records in the EASM region.

1. Introduction

Stalagmite $\delta^{18}O$ has been one of the most important proxies to track climate evolution during the late Quaternary in recent decades (e.g., Cheng *et al.* 2016, 2019). However, the interpretation of stalagmite $\delta^{18}O$ records from regions impacted by the Asian summer monsoon remains controversial. Wang *et al.* (2001) suggested that the evolution of $\delta^{18}O$ records in the east China stalagmite is driven predominantly by ratios of the summer and winter precipitation. Alternatively, Yuan *et al.* (2004) argued that variations in stalagmite $\delta^{18}O$ in the Dongge Cave were controlled mostly by the fraction of water vapour between the moisture sources and cave sites. Other views also suggested the contribution of various degrees of different moisture sources from the Indian and Pacific Oceans on the $\delta^{18}O$ signature (Maher & Thompson, 2012; Baker *et al.* 2015). Some studies noted that reconciling those factors may better explain the $\delta^{18}O$ of precipitation and stalagmites (Liu *et al.* 2014).

Pausata *et al.* (2011) suggested that Chinese stalagmite $\delta^{18}O$ was controlled by fluctuations in the Indian Summer Monsoon (ISM) intensity using climate model simulations for Heinrich stadial 1. They indicated that decreased intensity of the ISM results in enriched stalagmite $\delta^{18}O$ in eastern China during Heinrich stadial 1. Several geological archives have also recorded the contribution of the Indian Ocean to the $\delta^{18}O_P$ ($\delta^{18}O$ of precipitation) in eastern China (Yang *et al.* 2014; Chen *et al.* 2015; Liu *et al.* 2015). However, this viewpoint was challenged by other geological records (Tan, 2009; Tan, 2013; Li *et al.* 2019; Liang *et al.* 2020). For example, Tan *et al.* argued that moisture sources of the monsoon regions of China including both the Indian Ocean and the Pacific Ocean, with depleted and enriched $\delta^{18}O$ signal in precipitation (Tan, 2009, 2013). They found that the $\delta^{18}O$ signal in stalagmite reflects the intensity contrast between two

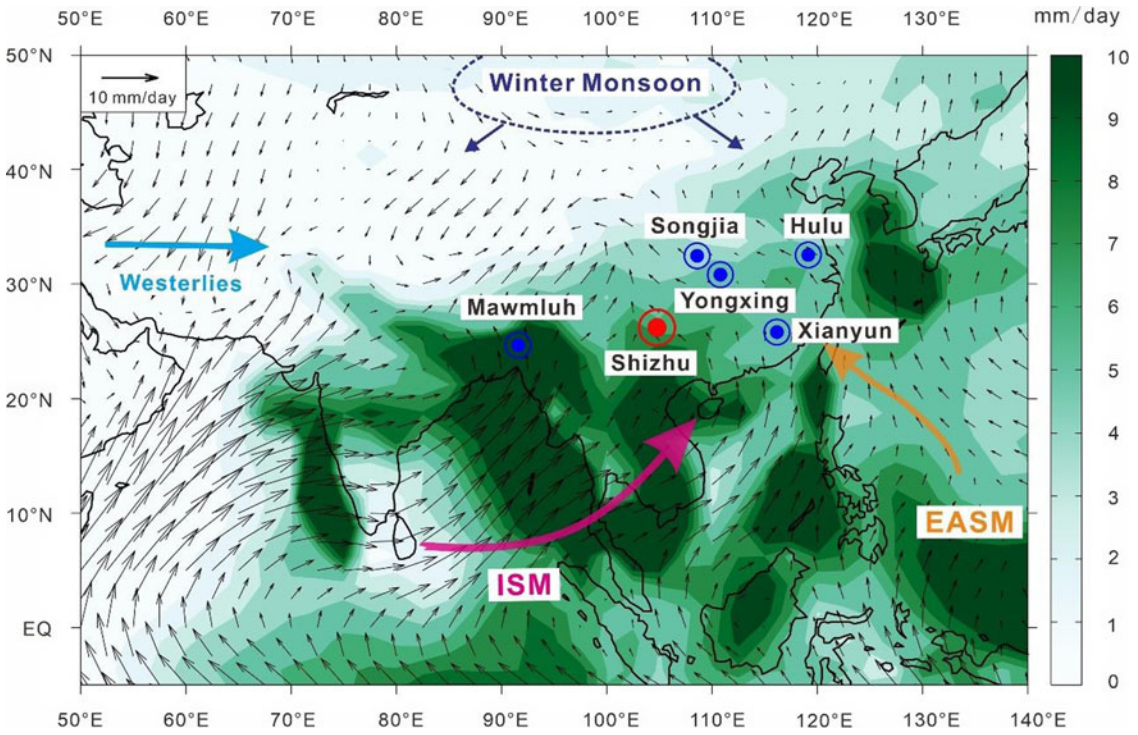

Figure 1. (Colour online) Cave locations in Asia. The detailed information for every cave is as follows: Mawmluh Cave: 25°15′N, 91°52′E, 1290 m a.s.l. (Dutt *et al.* 2015); Shizhu Cave: 26°02′N, 107°16′E, 950 m a.s.l. ; Xianyun Cave: 116°59′E, 25°33′N; 970 m a.s.l. (Zhang *et al.* 2021; Qiu *et al.* 2022); Hulu Cave: 32°32′N, 119°10′E, 90 m a.s.l. (Wang *et al.* 2001); Yongxing Cave: 31°35′N, 111°14′E, 750 m a.s.l. (Chen *et al.* 2016); Songjia Cave: 32°24′N, 107°10′E; 680 m a.s.l. (Zhou *et al.* 2008). The little black arrows represent the present-day averaged June–July–August (JJA) wind at 850 hPa (NCEP/NCAR, 1994). Four arrows represent the ISM, EASM, Westerly and Winter monsoon, respectively.

summer monsoons, the ISM and the East Asian Summer Monsoon (EASM), which is further dependent on the variation of the Western Pacific Subtropical High (WPSH). Li *et al.* (2019) subtracted the typical $\delta^{18}O$ signal of the ISM from a stalagmite record of eastern China during the Heinrich stadial 1 to isolate the Pacific's $\delta^{18}O$ signal. The latter signal shows a clear negative correlation with the Sea Surface Temperature (SST) of the Western Pacific Warm Pool.

Moreover, the position of the westerly jet in summer is also important in affecting stalagmite $\delta^{18}O$ records in China. The shifts of the westerly jet change the geographic position and $\delta^{18}O_P$ of the monsoon rainband (Sampe & Xie, 2010; Baker *et al.* 2015; Chiang *et al.* 2015, 2017, 2020). The rapid millennial-scale climatic changes during the last glacial occurred in the high-latitude Northern Hemisphere and transduced to East Asia, which is realized through the northern westerlies (e.g., Porter & An, 1995; Guo *et al.* 1996; Nagashima *et al.* 2011; Sun *et al.* 2012).

We suggest that systematic comparisons of the stalagmite $\delta^{18}O$ records at different spatial-temporal scales can help to resolve these disputes. The last glacial is the most recent period when global climate changed dramatically, with expanding ice sheet, lowering sea levels, exposing shelves (Siddall *et al.* 2003, 2008), dropping in SST (Kucera *et al.* 2005) and reorganizing in atmospheric–oceanic circulation (Bohm *et al.* 2015; Markle *et al.* 2016; Lynch-Stieglitz, 2017; Dong *et al.* 2022). In the Asian region, atmospheric–oceanic circulation changed, with a southward shift of the Intertropical Convergence Zone (ITCZ) in the South China Sea (Zhao *et al.* 2018; Kaboth-Bahr *et al.* 2021), weakened Asian summer monsoon (Cheng *et al.* 2012, 2016) and intensified winter monsoon (Sun *et al.* 2006, 2012).

Here, we established a high-resolution $\delta^{18}O$ record from two stalagmites of the Shizhu Cave from 45 to 15 ka B.P. in southwestern China (Fig. 1). The hydroclimate there is dominated by the ISM but also partly influenced by the EASM and the westerlies (Wang & Chen, 2012; Cai *et al.* 2015). Thus, stalagmites of the Shizhu Cave are suitable materials to better constrain the moisture trajectory of ISM in the past. Further, we compared $\delta^{18}O$ records of the Shizhu Cave with other available records that were widely deposited in the ISM and EASM regions during the middle to late last glacial to investigate the possible moisture trajectories of the Asian summer monsoon during this period. In this study, first, we explore the possible moisture trajectories over the ISM and EASM regions during the middle to late last glacial. Second, we obtain amplitudes of stalagmite $\delta^{18}O$ records from caves in the Asian region during Heinrich stadial 1 to 4 (HS1 to HS4) and investigate their distribution pattern to further discuss the controlling factors behind the pattern.

2. Materials and methods

2.a. Setting and sampling

The Shizhu Cave is located in the southern Guizhou Province (26°02′N, 107°28′E; 1089 m above sea level), southwestern China (Fig. 1). The mean annual temperature and precipitation are 16.1 °C and 1431.1 mm, respectively (http://data.cma.cn/dataService). Warm and humid air from the Indian Ocean and the equatorial Pacific Ocean generates heavy and continuous rain in this region from May to October, constituting about 80% of the yearly precipitation (Dykoski *et al.* 2005). Two stalagmites, SZ-1 and SZ-3 (Fig. 2), were sampled from the Shizhu Cave at a chamber approximately 50 m below the surface. SZ-1 and SZ-3 are 430 mm and 542.5 mm in length, respectively (Fig. 3).

https://doi.org/10.1017/S0016756824000013

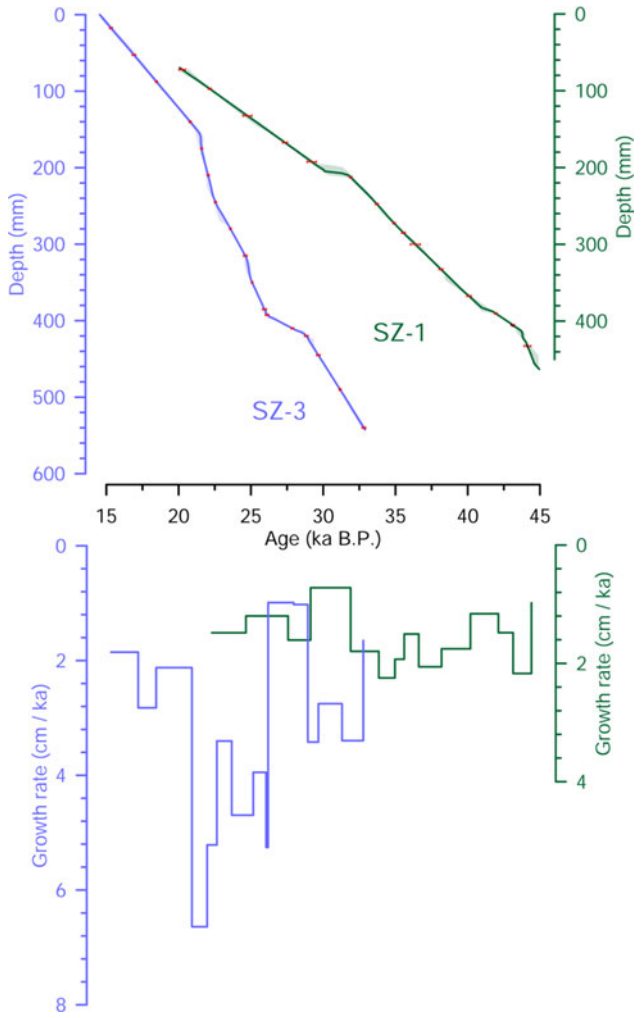

Figure 2. (Colour online) Age models and growth rates of the stalagmites SZ-1 and SZ-3 from Shizhu Cave. Age–depth relationship for SZ-1 (green line and axis) and SZ-3 (blue line and axis). Chronologies are established by U-Th dating and the StalAge model; error bars are indicated for every dating in red.

2.b. U-Th dating

The U-Th dating method is one of the most important advantages of stalagmite paleoclimate research because of its high degree of accuracy in absolute timing (Cheng *et al.* 2019). Thirty subsamples with 20 mm in length, 10 mm in width and 2.5 mm in depth were collected discontinuously from SZ-1 and SZ-3 along their growth axis for U-Th dating (Table 1). Uranium and thorium isotopic composition and content were measured using a multi-collector inductively coupled plasma mass spectrometer (MC-ICP-MS) in the High-Precision Mass Spectrometry and Environment Change Laboratory (HISPEC), Department of Geoscience, National Taiwan University (Shen *et al.* 2012). Uncertainties of the isotope data and U-Th dates, relative to 1950 AD, are given at the two-sigma (2s) level or two standard deviations of the mean ($2s_m$) unless otherwise noted. Decay constants used for age calculation are available in Cheng *et al.* (2013).

2.c. Oxygen isotopic measurements

The measurement technology of oxygen isotopes has been already quite mature after years of development. Here, 406 and 276 subsamples (cylinder of 0.3 mm diameter wide) were drilled, respectively, from the SZ-1 and SZ-3 with carbide dental burrs at a spacing of 2 mm along their growth axes. Acidic hydrolysis of $CaCO_3$ was then performed from the extracted material, to which 0.2 mg of calcite was added to each subsample, using H_3PO_4 at a concentration close to 100 % at a constant controlled temperature of ~72 °C to extract the CO_2. Released CO_2 was carried with helium (He) flow to an accessory Finnigan Gas Bench, where water vapour was separated through gas chromatography. The resultant CO_2 was ionized and accelerated to mass separation in an automated system. Measurements of oxygen and carbon stable isotopes were performed on a Gasbench attached to a Thermo MAT 253 mass spectrometer at Fujian Normal University with an external 1σ precision of ± 0.06‰. Oxygen isotope values were presented as $\delta^{18}O$ ($\delta^{18}O = [(^{18}O/^{16}O)_{sample}/(^{18}O/^{16}O)_{standard} - 1] \times 1000‰$) with the Vienna Pee Dee Belemnite (VPDB) standard.

2.d. X-ray diffraction (XRD) analysis

Calcite is more stable than other carbonate materials like aragonite in recording stable isotope information (Zhang *et al.* 2014). Thus, it is necessary to detect the properties of the research materials. Eight subsamples from the sectioned surfaces of the stalagmite SZ-1 and SZ-3 were collected for XRD analysis. For each subsample, 2 mg powder was loaded on stages with a silicon tablet background and analysed by a Rigaku MiniFlex benchtop X-ray diffraction (XRD) instrument (Cu-Kα radiation) in the Center for Social Science, Southern University of Science and Technology. The XRD spectra were obtained from 2° to 100° 2θ. The major phase identification and semi-quantification were conducted using the PDXL2 software.

2.e. Data collecting and statistical analysis

The stack curve between stalagmite $\delta^{18}O$ records of SZ-1 and SZ-3 in Figure 4 and the stack curve among five caves in Figure 7b were both obtained using the bootstrap resampling method, which can reserve the general trend of different curves as much as possible. Before stacking SZ-1 and SZ-3, we calculated the Pearson correlation coefficient between them in Fig. S1. The stack curve of SZ-1 and SZ-3 and the error bars are shown in Figure 4.

3. Results

3.a. Geochronology

The measured isotope ratios of U and Th, decay constants and calculated ages are listed in Table 1. Most of the 2σ uncertainties are better than 200 years for SZ-1 and 100 years for SZ-3, respectively. The StalAge chronology was used to establish the age models. Ages versus depths show that stalagmites SZ-1 and SZ-3 continuously grew from 45.0 to 22.0 ka B.P. and 32.8 to 14.4 ka B.P., respectively (Figs. 2 and 3). The growth rates vary from 1 to 7 cm/ka B.P. for SZ-1 and from 0.4 to 2.4 cm/ka B.P. for SZ-3. It is noted that samples before 22.28 ka B.P. of SZ-1 were lost before obtaining U-Th results, corresponding to a depth of about 0–9.75 cm. Thus, the $\delta^{18}O$ records before 22.28 ka are unusable.

3.b. XRD results

The XRD results (Fig. S2) indicate that samples from SZ-1 and SZ-3 are predominantly composed of calcite, which makes them suitable for studying oxygen isotope variations. It is noted that 'unclear laminations' occurring during the period 22.28 to 24.64 ka B.P. were observed in stalagmite SZ-1 (Fig. 3); they may be formed by the recrystallization of the primary calcite crystals, alter the

https://doi.org/10.1017/S0016756824000013

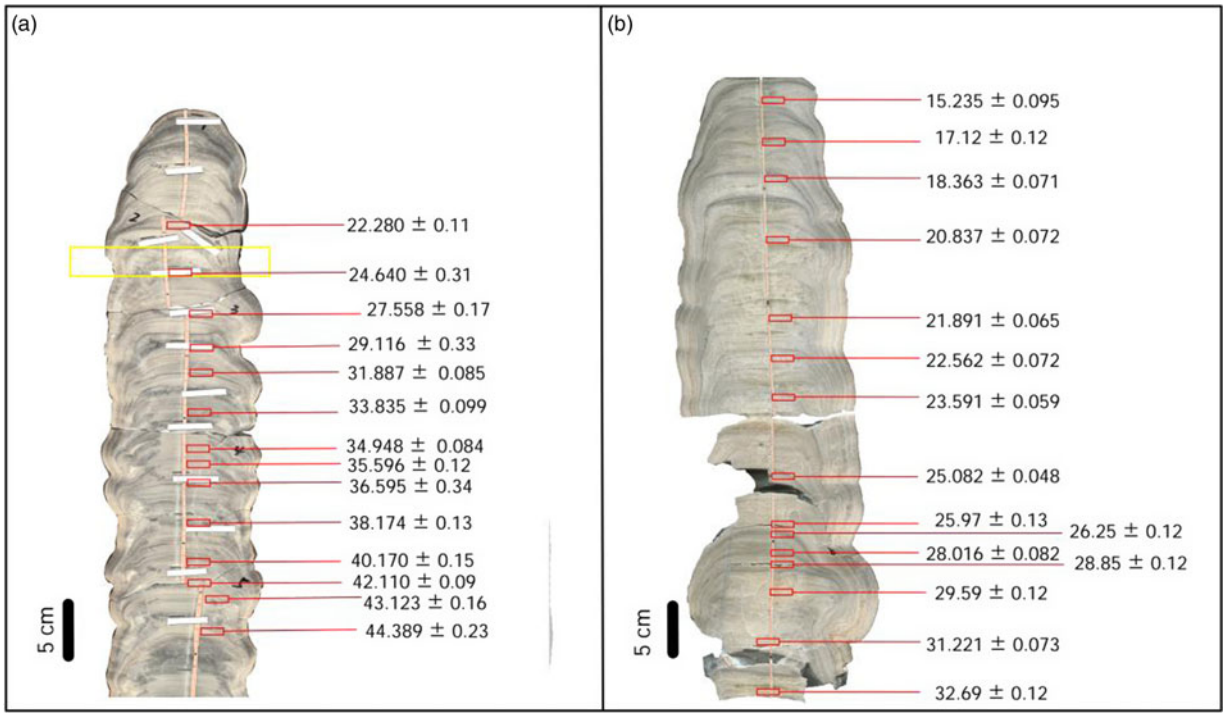

Figure 3. (Colour online) Cross sections of the stalagmites SZ-1 (a) and SZ-3 (b); the scale is the same for both stalagmites. The yellow rectangle in SZ-1 highlights the area where recrystallization might have occurred. Dating results and related dated areas of each stalagmite are indicated by the red rectangles. The white bars are remnants of the original marks and can be ignored. The oxygen isotope sampling track was performed directly on the left of the central axis of each stalagmite, which is marked by the orange lines.

primary stable isotope composition (Zhang *et al.* 2014; Lachniet, 2015) and thus have been excluded for further paleoclimate interpretations (Fig. 4a).

3.c. Combination of curve SZ-1-3

The $\delta^{18}O$ values of SZ-1 range between −2.31‰ and −7.87‰ with an average value of −5.50‰, while the $\delta^{18}O$ values of SZ-3 varied from −2.38‰ to −7.47‰ with an average value of −5.60‰. Centennial- to decadal-scale variability of SZ-1 and SZ-3 can be identified (Fig. 4), with averages of temporal resolution of 128 years (SZ-1) and 66 years (SZ-3). Although the evolution of $\delta^{18}O$ between SZ-1 and SZ-3 (Fig. 4c) could not overlap perfectly due to different growth rates and sampling resolutions during 32.65 to 24.64 ka B.P., their overall trend, amplitudes and the average value of variations are comparable. The result of the Pearson correlation coefficient in Fig. S1 is 0.56, indicating a medium correlation and implying that SZ-1 and SZ-3 are available for further stack analysis. We stacked these two curves deposited between 24.64 ka and 32.65 ka to composite SZ-1-3 with the error curves in Figure 4d. The centennial-scale amplitudes of SZ-1-3 are 2.53 ‰, 1.05 ‰, 0.96 ‰ and 2.86 ‰ at nearly 16 ka B.P., 24 ka B.P., 31 ka B.P. and 39 ka B.P., respectively, indicating the existence of HS1 to HS4 (Wang *et al.* 2001; Andersen, 2004). Additionally, the average values of SZ-1-3 during Marine Isotope Stages 2 and 3 (MIS 2 and MIS 3) are −5.16‰ and −5.56‰, respectively.

4. Discussion

4.a. The Asian stalagmite $\delta^{18}O$ records reveal moisture trajectories during the middle to late glacial

Previous studies have shown that variations in the stalagmite $\delta^{18}O$ indicate the mean state of summer monsoon intensity and/or the integrated moisture transports (Cheng *et al.* 2012, 2016). However, the exact mechanisms controlling the stalagmite $\delta^{18}O$ values are still widely debated, including the 'upstream depletion mechanism' (Yuan *et al.* 2004), the ratio of summer to winter rainfall (Wang *et al.* 2001) and the ratio of water vapour between the Pacific Ocean and the Indian Ocean (Tan, 2013). We suggest that systematic comparison at different spatial-temporal scales may partially settle those disputes. Then, we selected relatively continuous stalagmites $\delta^{18}O$ records from caves that are far enough to capture spatial variation in the Asian region during the middle to late last glacial for comparison.

The stalagmite $\delta^{18}O$ records in the monsoon region of China are controlled by $\delta^{18}O$ of yearly precipitation (Qiu *et al.* 2021), of which almost 80% is contributed by the EASM and the last 20% is dominated by the East Asian Winter Monsoon (EAWM) in the current climate setting. While, under the background of weakened Asian summer monsoon and intensified winter monsoon during the last glacial (Sun *et al.* 2006), this ratio may change partially. However, in this discussion, we do not explore the changed proportion emphasized by Wang *et al.* (2001) but focus on the averages of these stalagmite $\delta^{18}O$ records over the last glacial period.

Wang *et al.* (2001) explained the changed stalagmite $\delta^{18}O$ records of the Hulu Cave as the ratio between the East Asia summer and winter monsoon, which is very reasonable. Whereas, when comparing averages of stalagmite $\delta^{18}O$ records from different regions over the last glacial period, the enhanced winter winds had a relatively common effect on these caves, although the influences on these caves may differ. It is conceivable that summer precipitation still constitutes the majority of yearly precipitation (Jiang *et al.* 2011; Cai *et al.* 2015) and dominates the composition of stalagmite $\delta^{18}O$ records. Thus, the comparison among averages of stalagmite $\delta^{18}O$ records reflects summer moisture sources and

https://doi.org/10.1017/S0016756824000013

Table 1. U-Th isotopic measurements for Shizhu Cave stalagmite SZ-1 and SZ-3, on MC-ICP-MS

Sample	^{238}U		^{232}Th		$d^{234}U$		$[^{230}Th/^{238}U]$		$^{230}Th/^{232}Th$		Age (ka ago)		Age (ka ago)		$d^{234}U_{initial}$	
Length(cm)	$10^{-9}g/g$[a]		$10^{-9}g/g$		Measured[a]		Activity[c]		Atomic (x 10^{-6})		Uncorrected		Corrected[c,d]		Corrected[b]	
SZ1-9.75	2265.5	±2.7	7891.	±21	420.3	±1.6	0.2656	±0.0010	1257.2	±5.8	22.34	±0.10	22.28	±0.11	447.6	±1.7
SZ1-13.25	222.575	±0.042	6132.4	±4.1	412.00	±0.34	0.2943	±0.0014	176.11	±0.82	25.20	±0.13	24.64	±0.31	441.67	±0.53
SZ1-16.75	419.104	±0.049	6835.8	±5.2	401.65	±0.27	0.31982	±0.00051	323.30	±0.57	27.890	±0.050	27.56	±0.17	434.13	±0.36
SZ1-19.25	222.95	±0.26	5719	±16	413.1	±1.7	0.3398	±0.0022	218.4	±1.6	29.59	±0.23	29.12	±0.33	448.5	±1.9
SZ1-21.25	453.404	±0.060	3350.5	±2.5	419.95	±0.37	0.36618	±0.00041	817.0	±1.1	32.034	±0.043	31.887	±0.085	459.49	±0.42
SZ1-24.75	319.51	±0.41	148.1	±4.2	459.7	±2.0	0.39521	±0.00083	14062	±403	33.844	±0.099	33.835	±0.099	505.8	±2.2
SZ1-27.25	268.801	±0.062	1460.6	±2.3	425.61	±0.51	0.39759	±0.00062	1206.4	±2.7	35.056	±0.065	34.948	±0.084	469.73	±0.58
SZ1-28.5	247.687	±0.022	1345.4	±2	420.88	±0.33	0.4024	±0.0011	1221.5	±3.7	35.69	±0.11	35.60	±0.12	465.36	±0.40
SZ1-30.0	236.640	±0.045	6872.5	±7.3	422.37	±0.83	0.4166	±0.0021	236.5	±1.2	37.12	±0.22	36.60	±0.34	468.3	±1.0
SZ1-33.25	295.01	±0.37	285.9	±2.1	431.27	±1.95	0.42960	±0.00106	7309	±55	38,191	±128.04	38,174	±128	480.32	±2.18
SZ1-36.75	253.70	±0.32	571.5	±2.2	439.72	±2.02	0.45151	±0.00125	3305	±15	40,210	±149.38	40,170	±151	492.51	±2.27
SZ1-39	3459.60	±0.93	27919.0	±33.8	435.56	±0.51	0.46926	±0.00047	959	±1	42,253	±53.81	42,110	±90	490.52	±0.59
SZ1-40.5	234.75	±0.05	221.6	±2.2	443.43	±0.51	0.48017	±0.00166	8386	±87	43,138	±180.13	43,121	±180	500.81	±0.63
SZ1-43.25	280.79	±0.40	1907.6	±4.0	451.75	±2.36	0.49576	±0.00187	1203	±5	44,508	±221.92	44,389	±229	512.04	±2.70
SZ3-1.75	672.65	±0.97	4027.0	±8.3	795.7	±3.1	0.2386	±0.0012	657.2	±3.4	15.391	±0.085	15.235	±0.095	830.9	±3.2
SZ3-5.25	676.3	±1.0	5737.0	±9.9	778.5	±3.0	0.2639	±0.0013	513.0	±2.6	17.316	±0.099	17.12	±0.12	817.2	±3.1
SZ3-8.75	844.1	±1.1	2227.7	±4.2	798.8	±2.7	0.28348	±0.00087	1771.1	±6.0	18.470	±0.068	18.363	±0.071	841.5	±2.8
SZ3-14.0	869.8	±1.2	1129.1	±3.0	742.2	±3.2	0.30798	±0.00078	3912	±13	20.925	±0.072	20.837	±0.072	787.3	±3.4
SZ3-21.0	911.7	±1.4	220.6	±2.0	722.7	±3.1	0.31831	±0.00063	21696	±195	21.964	±0.065	21.891	±0.065	768.9	±3.3
SZ3-24.5	910.6	±1.0	2003.7	±4.0	714.1	±2.1	0.32590	±0.00083	2442.0	±7.5	22.664	±0.070	22.562	±0.072	761.2	±2.2
SZ3-28.0	933.1	±1.3	169.6	±2.2	705.6	±2.5	0.33723	±0.00058	30588	±406	23.663	±0.059	23.591	±0.059	754.3	±2.7
SZ3-35.0	1104.2	±1.1	281.6	±2.1	687.8	±1.7	0.35266	±0.00049	22802	±169	25.155	±0.048	25.082	±0.048	738.4	±1.9
SZ3-38.5	891.05	±0.96	5684	±10	690.5	±2.0	0.3656	±0.0015	945.0	±4.1	26.13	±0.12	25.97	±0.13	743.2	±2.1
SZ3-39.25	828.71	±0.13	9661	±10	686.81	±0.41	0.36758	±0.00094	519.9	±1.4	26.358	±0.075	26.25	±0.12	739.48	±0.50
SZ3-41.0	704.98	±0.10	7170.3	±9.4	627.78	±0.33	0.37541	±0.00018	608.57	±0.84	28.107	±0.016	28.016	±0.082	679.30	±0.39
SZ3-42.0	788.20	±0.84	3592.0	±5.7	617.1	±2.0	0.3834	±0.0012	1387.0	±4.8	29.00	±0.11	28.85	±0.12	669.6	±2.1
SZ3-44.5	778.91	±0.81	3513.7	±6.4	641.8	±1.8	0.3980	±0.0013	1454.8	±5.4	29.73	±0.12	29.59	±0.12	697.8	±2.0
SZ3-49.0	889.45	±0.98	116.8	±2.5	653.4	±1.9	0.41952	±0.00070	52681	±1117	31.292	±0.073	31.221	±0.073	713.7	±2.1
SZ3-54.0	950.4	±1.7	558.1	±2.2	651.1	±3.3	0.4362	±0.0011	12248	±54	32.77	±0.12	32.69	±0.12	714.1	±3.6

Analytical errors are 2s of the mean.

[a] $[^{238}U] = [^{235}U] \times 137.818$ (±0.65‰) (Hiess *et al.* 2012); $d^{234}U = ([^{234}U/^{238}U]_{activity} - 1) \times 1000$.

[b] $d^{234}U_{initial}$ corrected was calculated based on ^{230}Th age (T), i.e., $d^{234}U_{initial} = d^{234}U_{measured} \times e^{\lambda 234 \cdot T}$, and T is corrected age.

[c] $[^{230}Th/^{238}U]_{activity} = 1 - e^{-\lambda 230 T} + (d^{234}U_{measured}/1000)[\lambda_{230}/(\lambda_{230} - \lambda_{234})](1 - e^{-(\lambda 230 - \lambda 234) T})$, where T is the age.

Decay constants are 9.1705×10^{-6} yr^{-1} for ^{230}Th, 2.8221×10^{-6} yr^{-1} for ^{234}U (Cheng *et al.* 2013) and 1.55125×10^{-10} yr^{-1} for ^{238}U (Jaffey *et al.* 1971).

[d] Age corrections, relative to chemistry date, were calculated using an estimated atomic $^{230}Th/^{232}Th$ ratio of 4 (± 2) $\times 10^{-6}$.

Those are the values for material at secular equilibrium, with the crustal $^{232}Th/^{238}U$ value of 3.8. The errors are arbitrarily assumed to be 50%.

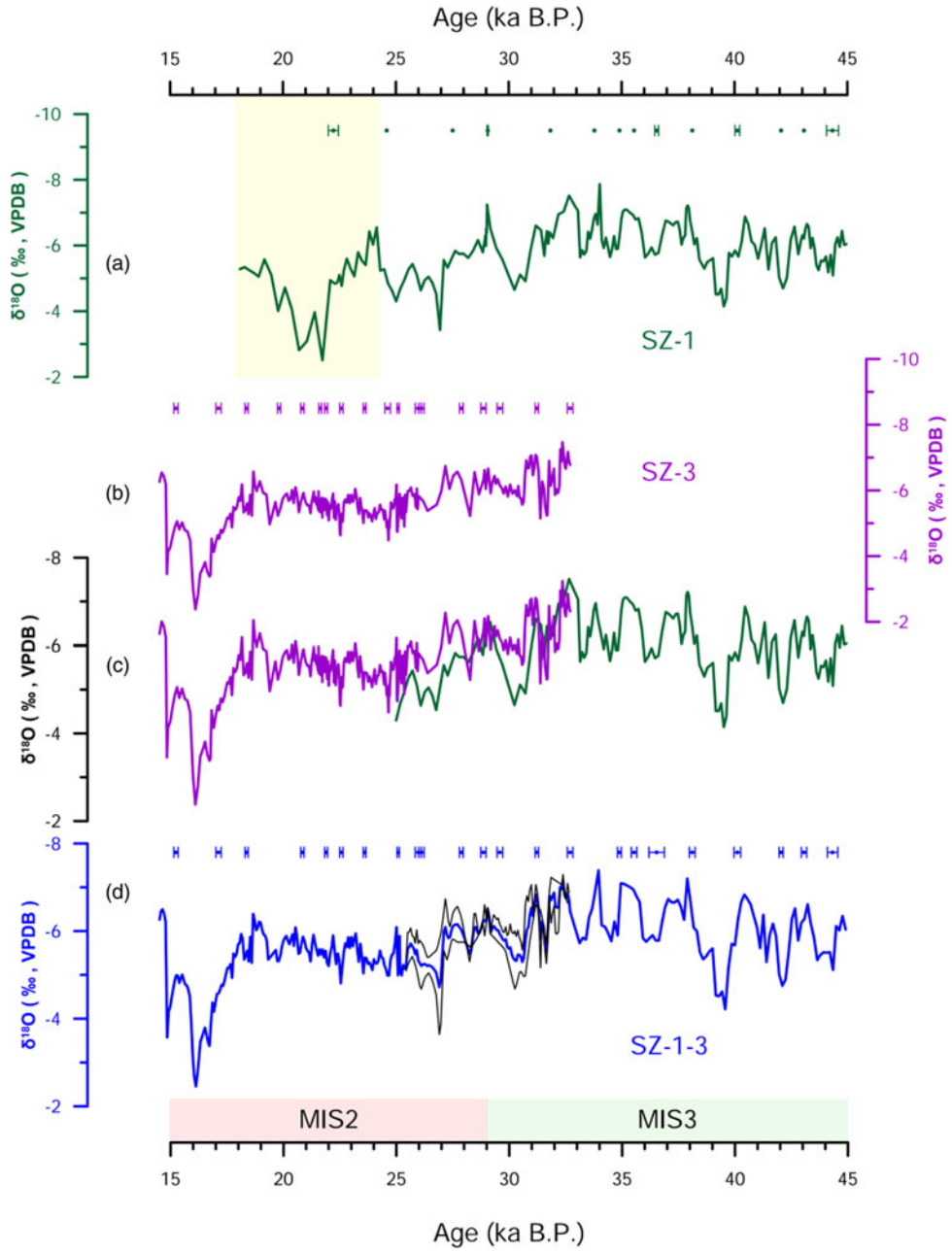

Figure 4. (Colour online) $\delta^{18}O$ records from the stalagmites SZ-1 and SZ-3 investigated in this study. The original $\delta^{18}O$ records from (a) SZ-1 (forest green) and (b) SZ-3 (purple). (d) Composite Shizhu $\delta^{18}O$ record SZ-1-3 (navy blue). Error bars of the ^{230}Th dating points are shown at the top for both stalagmites. The light yellow bar in (a) highlights the stage lacking dating results before 22.28 ka and the possible recrystallization during 22.28 ka to 24.64 ka B.P. of SZ-1. The black lines in (d) are error curves of stack analysis. The light pink and green rectangles present the periods of MIS 2 and MIS 3.

trajectories during the middle to late last glacial period based on Rayleigh fractionation (Dansgaard, 1964).

Hu *et al.* (2008) compared stalagmite $\delta^{18}O$ records from two caves along the same moisture transport path to quantify the history of rainfall during the Holocene, verifying the effectiveness of comparing records from different regions based on spatially coherent variability. Further, Li *et al.* (2017) demonstrated the different moisture sources and paths of southwest and east China by comparing stalagmite $\delta^{18}O$ records from different regions. In the ISM region, the spatial variation of stalagmite $\delta^{18}O$ records from coast to inland has been demonstrated on a subregional scale in south and Southeast Asia by Liu *et al.* (2020) over the past 40 ka. In the EASM region, Zhang *et al.* (2021) demonstrated that the Yongxing Cave was located downstream of the EASM moisture path during the last glacial. These previous studies inspire us but lack systematical comparison on larger spatial scales.

The graph in Figure 5 illustrates how the average isotope values change over time. The Shizhu Cave is located at the main path of the ISM moisture trajectory whether in the present day or during the last glacial (Fig. 1; Fig. 6). Therefore, SZ-1-3 records are used to compare with those from sites along the ISM moisture trajectory (i.e., Mawmluh and Yongxing Caves) between 45 and 15 ka B.P. (Fig. 5). Their average values in Figure 5a show systematically decrease from the Indian Ocean to inland China. Specifically, the

https://doi.org/10.1017/S0016756824000013

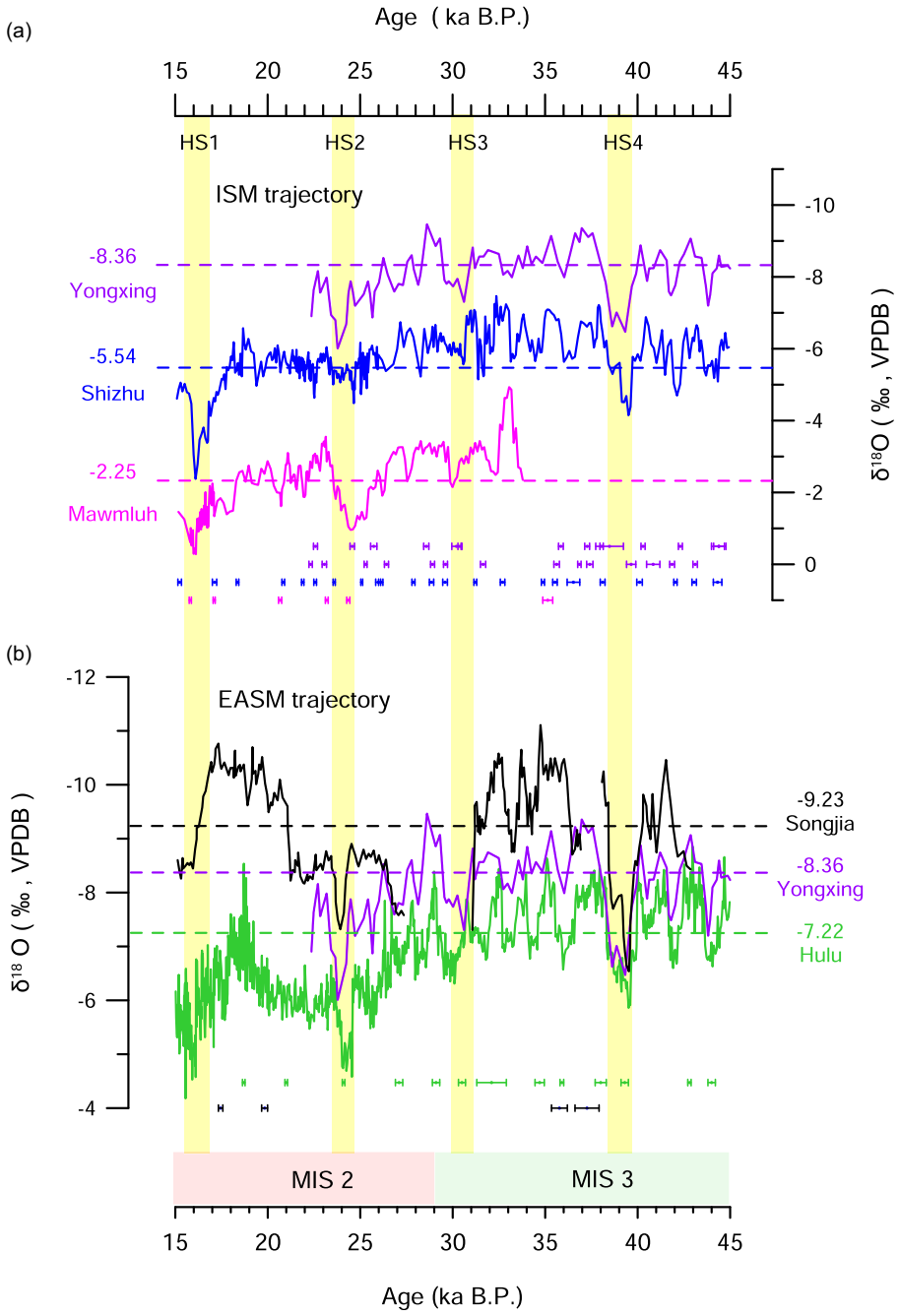

Figure 5. (Colour online) Comparison of $\delta^{18}O$ records on ISM and EASM moisture trajectories. (a) Mawmluh (pink), Shizhu (navy blue; this study) and Yongxing (purple) Cave records. (b) Hulu (green), Yongxing (purple) and Songjia (black) Cave records. The light yellow bars highlight the four weak monsoon periods in the Asian monsoon regions, coeval with the Heinrich stadials 1 to 4 (Wang *et al.* 2001). The light pink and green rectangles are the same as in Figure 4.

stalagmite $\delta^{18}O$ records of Mawmluh Cave are significantly enriched because it is close to the moisture source, the Indian Ocean (Dutt *et al.* 2015). In contrast, the $\delta^{18}O$ records in the Yongxing Cave are considerably lower than those of the Shizhu and Mawmluh Caves because of its midstream or downstream location along the moisture trajectory of the ISM (yellow arrows in Figure 6; Hu *et al.* 2008; Cai *et al.* 2015; Chen *et al.* 2016). We demonstrate here that water vapour fractionation along this coastal-inland moisture transport route from the Indian Ocean to the coastal Mawmluh Cave, then to the Shizhu Cave, and probably extended to the Yongxing Cave during 45 and 15 ka (Fig. 6).

In the eastern monsoonal region of China, the coastal Xianyun and Hulu Caves received more enriched $\delta^{18}O$ of precipitation from the adjacent tropical and western Pacific Oceans (Wang *et al.* 2001; Zhang *et al.* 2021; Qiu *et al.* 2022). From the coastal Hulu/Xianyun Caves to the western inland Yongxing and then Songjia Caves, the average stalagmite $\delta^{18}O$ values gradually decrease (Fig. 5b). We suggest that water vapour fractionation along this coastal-inland moisture transport route from the Pacific Ocean to the Yongxing Cave can be extended to the Songjia Cave during 45 and 15 ka (orange arrows in Fig. 6). Additionally, from coastal Hulu/Xianyun Caves to Dragon records in northern China (Dong *et al.* 2018) probably imply a northern moisture trajectory. Overall, we propose that the two moisture trajectories from the Indian Ocean and the Pacific Ocean may exist during 45–15 ka B.P., just as similar to the climatology of modelled summer water vapour transport during the last glacial period (Cai *et al.* 2015; Fig. 6).

https://doi.org/10.1017/S0016756824000013

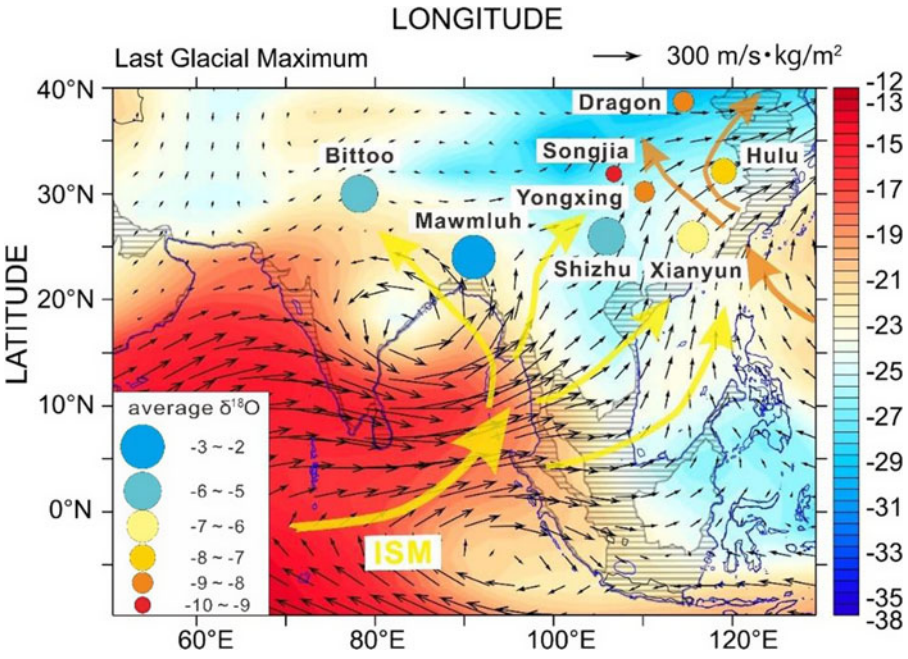

Figure 6. (Colour online) Possible ISM (yellow arrows) and EASM (orange arrows) moisture trajectories during the middle to late last glacial. The base map is modified from Cai *et al.* (2015), showing modelled June–August vapour transport (arrows, $m^{-1}skgm^{-2}$) and isotopic composition of column integrated vapour (colour-shading, ‰) during the last glacial maximum. Dark grey lines indicate the present coastline; the blue lines and hatched area indicate the coastline and the exposed continental shelf during the LGM when the sea level was ~120 m lower than the present day. Legends in the left bottom indicate distribution intervals of the averages of stalagmite $\delta^{18}O$ records during the middle to late last glacial.

4.b. Spatial pattern of millennial-scale variations of Asian stalagmite $\delta^{18}O$ records

Millennial-scale abrupt climate changes also occur during 45–15 ka B.P., that is, Heinrich stadials. To highlight these Heinrich stadials, the Hulu, Yongxing, Dragon, Mawmluh and Shizhu $\delta^{18}O$ records in the Asian region in Figure 7a were selected according to their data availability during the middle to late last glacial and far distances among them. We highlighted their changes during HS1 to HS4 after minus their respective averages of $\delta^{18}O$ records in Figure 7a. We further stacked them using the bootstrap resampling method to avoid visual clutter in Figure 7b. The stacked curve shows rather consistent changes during HS1 to HS4. This consistent strongly suggests that they are dominated simultaneously by the same mechanism – integral changes in atmospheric–oceanic circulation patterns of the East Asian Monsoon (Wang *et al.* 2001), which is further linked to the paleoclimatic changes in the North Atlantic region (Fig. 7c, d).

Abrupt cooling at the North Atlantic region during the Heinrich stadials presents a north–south propagation of climatic signal initiated by the intrusion of vast amounts of freshwater into the Atlantic from melting continental ice sheets, which have been proved by Ice Raft Debris (IRD in Fig. 7c). This causes a disruption of the meridional overturning circulation (Bohm *et al.* 2015; Markle *et al.* 2016; Lynch-Stieglitz, 2017; Dong *et al.* 2022) and further a reduction of the northward heat transport, leading to a cooling in the middle and high-latitude North Atlantic (Fig. 7d) and warming of the Southern Hemisphere (Zhang & Delworth, 2005). This distinct change in heat balance between both hemispheres causes anomalously southward migration of the ITCZ (Chiang & Bitz, 2005; Broccoli *et al.* 2006), severely altering the spatial precipitation pattern in the tropics and subtropics (Jacobel *et al.* 2016), including the Asian summer monsoon region.

Specifically, the Asian summer monsoon consists of tropical ISM and hybrid EASM, which in response to Heinrich stadials different in detail. From the perspective of ISM, the ITCZ shifts southward, leading to a relatively dry and cool climate over the northern Indian Ocean (Dahl *et al.* 2005; Clement & Peterson, 2008; Mohtadi *et al.* 2014; Zorzi *et al.* 2015; Tierney *et al.* 2016; Bradley *et al.* 2017) and decreasing rainfall and river runoff in the south Asian subcontinent further (Mohtadi *et al.* 2014; Deplazes *et al.* 2014). Simulations also show that the sudden increase in North Atlantic sea-ice extent in the HS1 impacts the Indian Ocean climate and causes a sudden increase in $\delta^{18}O_P$ over the Indian subcontinent, as well as isotopically heavier water vapour exported eastward into Southeast Asia (Pausata *et al.* 2011).

Overall, it is commonly agreed that climate changes in the Indian Ocean are the primary cause of enriched stalagmite $\delta^{18}O$ records in the ISM regions from HS1 to HS4. The change in water vapour in the Indian Ocean and the Indian subcontinent to what extent affects the EASM region is still controversial. As described above, Pausata *et al.* (2011) proposed that the changed water vapour in the Indian Ocean leads to enriched $\delta^{18}O_P$ in the ISM region. These two mutually account for $\delta^{18}O_P$ of the downstream EASM region. That is to say, variations of stalagmite $\delta^{18}O$ records in Chinese caves during Heinrich stadials are almost entirely affected by the ISM rather than the EASM.

However, recent studies suggest that the meridional position of the westerlies also affects the precipitation seasonality, and consequently, the $\delta^{18}O$ of precipitation and stalagmite records in the EASM region (Chiang *et al.* 2015, 2017, 2020; Liang *et al.* 2020). For example, Liang *et al.* (2020) suggested that 28°N is a boundary line for stalagmite $\delta^{18}O$ records, with higher amplitude in the north (>1.5‰) and lower amplitude in the south (~1‰) during HS1. The impediment of the westerly jet stream caused a small fraction of maritime moisture transported into inland China (less $\delta^{18}O$-depleted precipitation), but a large fraction (more $\delta^{18}O$-depleted precipitation) can still reach the lower latitude regions under modern settings and the Heinrich stadials. Thus, a mixture of yearly rainfall could cause small amplitude changes in calcite $\delta^{18}O$ and regional differences in the north and south of the boundary line.

Furtherly, to detect factors affecting stalagmite $\delta^{18}O$ records in the EASM region, we took amplitudes, which are defined as the departures apart from the background, of existing stalagmite $\delta^{18}O$

https://doi.org/10.1017/S0016756824000013

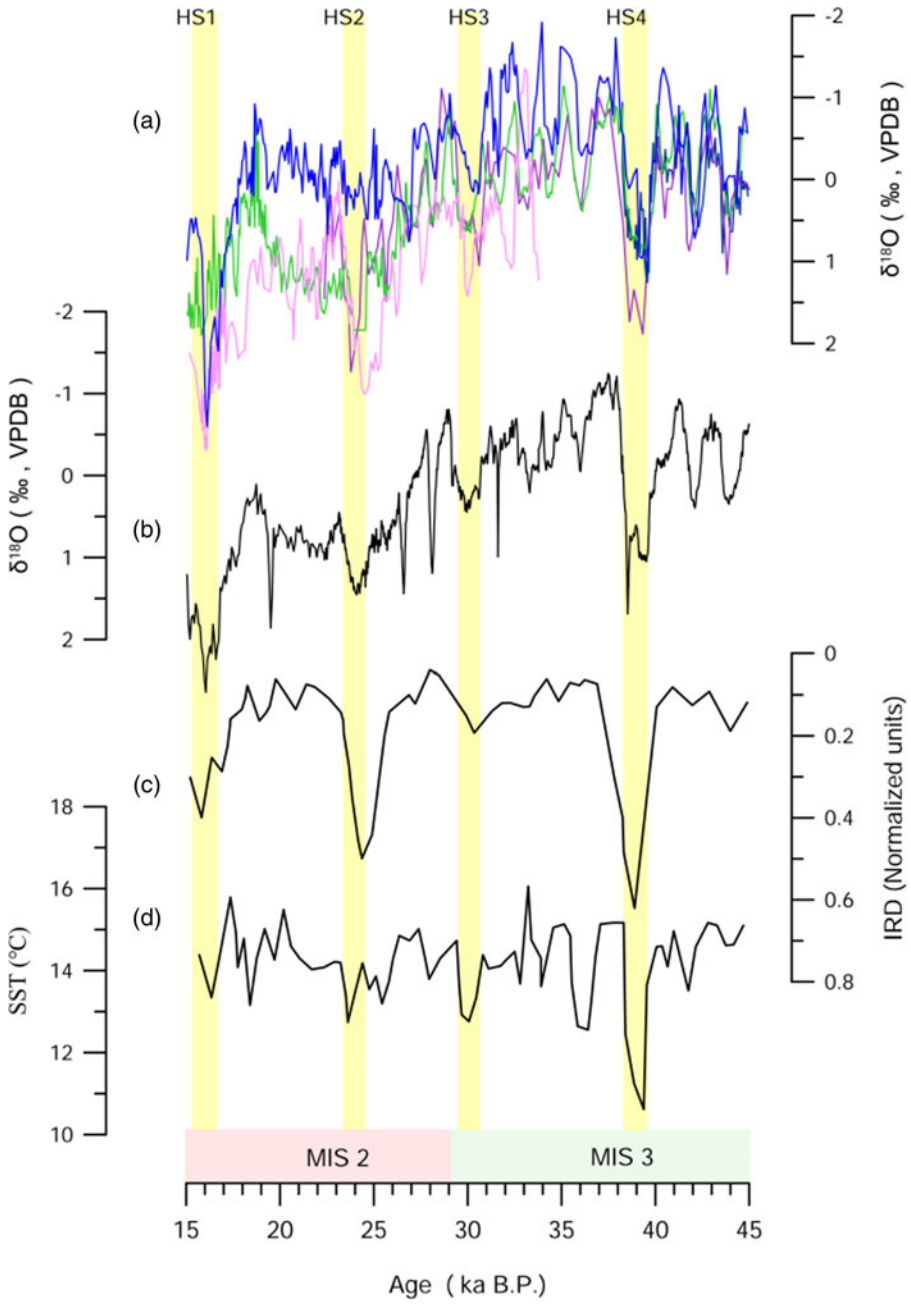

Figure 7. (Colour online) Response of stalagmite $\delta^{18}O$ records to IRD and SST in North Atlantic. (a) Rcords from the Mawmluh, Shizhu, Yongxing, Hulu and Dragon Caves after minus their respective average values; (b) the stacked curve of these five caves which is calculated by bootstrap resampling method; (c–d) IRD and SST records are referred to Lisiecki & Stern (2016).

records (shown in Fig. S3) widely in Asian summer monsoon during HS1 to HS4 for comparison by the method in Fig. S4. As shown in Tab. S1 and Figure 8, amplitudes of stalagmite $\delta^{18}O$ records from different caves increase from coastal oceans to mid-latitude inland China, presenting a 'coastal-inland' pattern, which is probably associated with two types of explanations.

First, this is possibly interpreted by the increased continental climate in central China, which concerns decreased summer rainfall amounts. Changing North Atlantic surface water strengthens the EAWM and weakens the summer monsoon probably through the northern westerlies (Porter & An, 1995; Sun *et al.* 2012). The southern shifts of the ITCZ in the tropical ocean (Mohtadi *et al.* 2014) and the South China Sea (Kaboth-Bahr *et al.* 2021) together with exposed shelves in the Asian region caused less maritime moisture transported into inland China, which means less $\delta^{18}O$-depleted precipitation in a year as Wang *et al.* (2001) proposed. Chiang *et al.* (2015) also suggested that a southward movement of the westerly jet could prevent the inland intrusion of the low-level monsoonal flow and Asian summer monsoon moisture. Eventually, the summer seasonality is gradually reducing in central China with increasing distance to oceans, resulting in increasing amplitudes of stalagmite $\delta^{18}O$ records during Heinrich stadials.

Another possibility is the increased proportion of summer moisture resources from the Pacific Ocean. Tan (2009, 2011, 2013, 2016) proposed that the position of the WPSH affects this proportion in summer monsoonal China. The WPSH is further associated with the global atmospheric and oceanic circulation. Specifically, a strong WPSH at a more southwestern location may weaken the ISM over the Bay of Bengal and strengthen the EASM over the South China Sea and the Western North Pacific, and vice versa (e.g., Gong & Ho, 2002; Zhou *et al.* 2009; Cao *et al.* 2012,

https://doi.org/10.1017/S0016756824000013

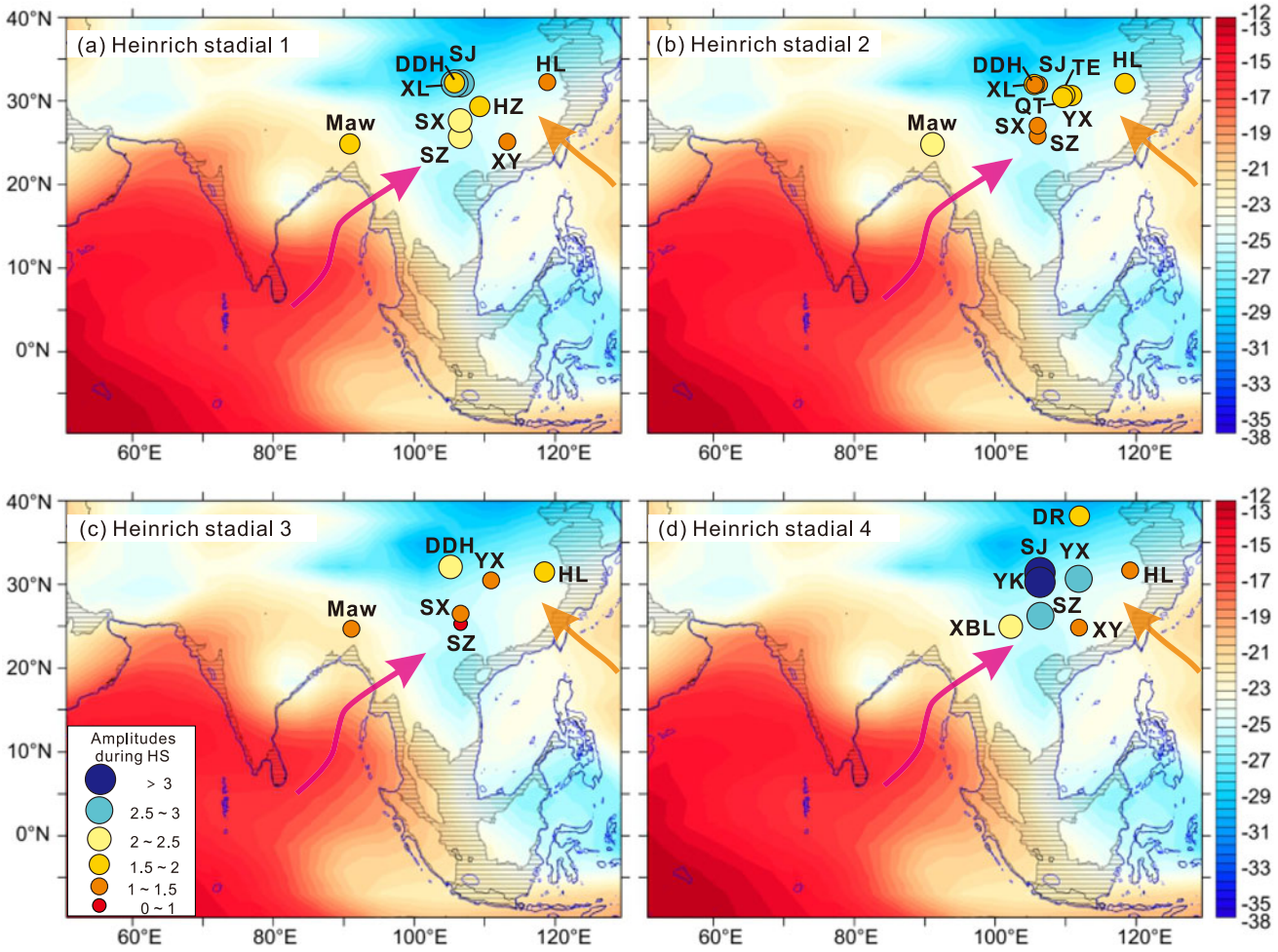

Figure 8. (Colour online) Changing amplitudes of caves during Heinrich stadials 1 to 4. The pink and orange arrows indicate the positions of ISM and EASM. The information on the base map is the same as in Figure 6.

2016). The enriched stalagmite $\delta^{18}O$ records of caves in southeast China during HS1 to HS4 were possibly caused by an increased proportion of moisture from the Pacific Ocean. As to the 'coastal-inland' pattern, Zhao *et al.* (2019) proposed that caves in other monsoon regions of China with dominant moisture sources from either the Pacific or the Indian Ocean are not significantly correlated with WPSH variations. Considering this, we suggest that the caves located in central China where influenced by both ISM and EASM are most affected by the changed proportion, showing the biggest amplitudes in the southeast China region during Heinrich stadials.

Additionally, the distribution pattern of HS2 (Fig. 8b) seems to differ from the last three, without an obvious 'coastal-inland' pattern. While records in the EASM region in Figure 8b show a less obvious 'south-north' pattern in mid-low latitudes. Some researchers suggest that this pattern is possibly caused by the migration of the westerlies during Heinrich stadials directly (Chiang *et al.* 2015, 2017, 2020; Nagashima *et al.* 2011). The specific mechanisms have been described above by the Liang *et al.* (2020). Besides, it is noted that the Dragon Cave in northern China in Figure 8d presents smaller amplitudes, compared with these caves in central China. A previous study of backward trajectory analysis in northern China reveals the importance of westerly borne and near-sourced moisture, dominating 77% of the summertime rainfall (Draxler & Hess, 1998). This probably leads to a weaker source effect and smaller amplitudes of the Dragon Cave during Heinrich stadials compared with caves in central China.

Conclusion

To further explore the moisture transportation process from oceans to the continent over China in the past, we present stalagmite $\delta^{18}O$ records between 45 and 15 ka B.P. from the Shizhu Cave, southwestern China. After comparing it with other Asian $\delta^{18}O$ records, we propose two main moisture trajectories: one from the Indian Ocean, through the Shizhu Cave to central China, and one from the Pacific Ocean to central China. This gradually systematical decreasing average values of stalagmite $\delta^{18}O$ from oceans to inland China present a spatial pattern of water vapour fractionation during the middle to late last glacial. Further, to explore factors affecting stalagmite $\delta^{18}O$ records in the EASM region during Heinrich stadials, we took amplitudes of stalagmite $\delta^{18}O$ records widely in Asian summer monsoon during HS1 to HS4 for comparison. The amplitude results show an increasing trend from coastal oceans to mid-latitude inland China, presenting a

https://doi.org/10.1017/S0016756824000013

'coastal-inland' pattern, which is probably associated with the decreased summer rainfall amount in inland areas or/and the increased proportion of summer moisture resources from the Pacific Ocean.

Supplementary material. To view supplementary material for this article, please visit https://doi.org/10.1017/S0016756824000013

Acknowledgements. This research was supported by grants from the National Natural Science Foundation of China (42074071, 42071106, 41874078, 92158208, 42274094), Shenzhen Science and Technology Program (grant no. KQTD20170810111725321), Science and Technology Innovation Committee of Shenzhen Municipality (ZDSYS201802081843490), Technology and Innovation Commission of Shenzhen Municipality (20200925154739001), Southern University of Science and Technology (Y01316111), and Key Special Project for Introduced Talents Team of Southern Marine Science, the International Cooperation Project of Fujian (2022I0013 to X. J) and Engineering Guangdong Laboratory (Guangzhou) (GML2019ZD0210). U-Th dating was partially supported by grants from the National Science and Technology Council (111-2116-M-002-022-MY3), the National Taiwan University (112L894202 to C.-C.S.), and the Higher Education Sprout Project of the Ministry of Education (110L901001 and 110L8907). Shanghai Sheshan National Geophysical Observatory (SSKP202102).

Competing interests. We declare that we have no financial and personal relationships with other people or organizations that can inappropriately influence our work, and there is no professional or other personal interest of any nature or kind in any product, service, and/or company that could be construed as influencing the position presented in, or the review of, the manuscript entitled, '**Chinese stalagmite $\delta^{18}O$ records reveal the diverse moisture trajectories during the middle to late last glacial period**'.

References

Andersen KK (2004) High-resolution record of northern hemisphere climate extending into the last interglacial period. *Nature* **431**, 147–51.

Baker AJ, Sodemann H, Baldini JUL, Breitenbach SFM, Johnson KR, Hunen JV and Zhang PZ (2015) Seasonality of westerly moisture transport in the East Asian summer monsoon and its implications for interpreting precipitation $\delta^{18}O$. *Journal of Geophysical Research: Atmospheres* **120**, 5850–62.

Bohm E, Lippold J, Gutjahr M, Frank M, Blaser P, Antz B, Fohlmeister J, Frank N, Andersen MB and Deininger M (2015) Strong and deep Atlantic meridional overturning circulation during the last glacial cycle. *Nature* **517**, 73–6.

Bradley RM, Eric JS, Christo B, Spruce WS, Cecilia MB, Fudge TJ, Joel BP, Ding QH, Tyler RJ, Jones WCW and Todd S (2017) Global atmospheric teleconnections during Dansgaard-Oeschger events. *Nature Geoscience* **10**, 36–40.

Broccoli AJ, Dahl KA and Stouffer RJ (2006) Response of the ITCZ to Northern Hemisphere cooling. *Geophysical Research Letters* **33**, L01702.

Cai YJ, Fung IY, Edwards RL, An ZS, Cheng H, Lee JE, Tan LC, Shen C-C, Wang XF, Day JA, Zhou WJ, Kelly MJ and Chiang JC (2015) Variability of stalagmite-inferred Indian monsoon precipitation over the past 252,000 y. *Proceedings of the National Academy of Sciences of the United States of America* **112**, 2954–9.

Cao J, Gui S, Su Q and Yang Y (2016) The variability of the Indian-East Asian summer monsoon interface in relation to the spring seesaw mode between the Indian Ocean and the central-western Pacific. *Journal of Climate* **29**, 5027–40.

Cao J, Hu J and Tao Y (2012) An index for the interface between the Indian summer monsoon and the East Asian summer monsoon. *Journal of Geophysical Research: Atmospheres* **117**, 108.

Chen FH, Chen XM, Chen JH, Zhou AF, Wu D, Tang LY, Zhang XJ, Huang XZ and Yu JQ (2015) Holocene vegetation history, precipitation changes, and Indian summer monsoon evolution documented from sediments of Xingyun Lake, southwest China. *Journal of Quaternary Science* **29**, 661–74.

Chen ST, Wang YJ, Cheng H, Edwards RL, Wang XF, Kong XG and Liu DB (2016) Strong coupling of Asian Monsoon and Antarctic climates on suborbital timescales. *Scientific Report* **8**, 32995.

Cheng H, Edwards RL, Shen C-C, Polyak VJ, Asmerom Y, Woodhead J, Hellstrom J, Wang YJ, Kong XG, Spötl C, Wang XF and Alexander JEC (2013) Improvements in ^{230}Th dating, ^{230}Th and ^{234}U half-life values, and U-Th isotopic measurements by multi-collector inductively coupled plasma mass spectrometry. *Earth and Planetary Science Letters* **371–372**, 82–91.

Cheng H, Edwards RL, Sinha A, Spötl C, Yi L, Chen ST, Kelly M, Kathayat G, Wang XF, Li XL, Kong XG, Wang YJ, Ning YF and Zhang HW (2016) The Asian monsoon over the past 640,000 years and ice age terminations. *Nature* **534**, 640–6.

Cheng H, Sinha A, Wang XF, Cruz FW and Edwards RL (2012) The Global Paleomonsoon is seen through speleothem records from Asia and the Americas. *Climate Dynamics* **39**, 1045–62.

Cheng H, Zhang HW, Zhao JY, Li HY, Ning YF and Kathayat G (2019) Chinese stalagmite paleoclimate researches: a review and perspective. *Science China Earth Sciences* **62**, 1–25.

Chiang JCH and Bitz CM (2005) Influence of high latitude ice cover on the marine Intertropical Convergence Zone. *Climate Dynamics* **25**, 477–96.

Chiang JCH, Fung IY, Wu CH, Cai YJ, Edman JP, Liu YW, Day JA, Bhattacharya T, Mondal Y and Labrousse CA (2015) Role of seasonal transitions and westerly jets in East Asian paleoclimate. *Quaternary Science Reviews* **108**, 111–29.

Chiang JCH, Herman MJ, Yoshimura K and Fung IY (2020) Enriched East Asian oxygen isotope of precipitation indicates reduced summer seasonality in regional climate and westerlies. *Proceedings of the National Academy of Sciences of the United States of America* **117**, 14745–50.

Chiang JCH, Swenson LM and Kong W (2017) Role of seasonal transitions and the westerlies in the interannual variability of the East Asian summer monsoon precipitation. *Geophysical Research Letters* **44**, 3788–95.

Clement AC and Peterson LC (2008) Mechanisms of abrupt climate change of the last glacial period. *Reviews of Geophysics* **46**, RG4002, 1–39.

Dahl KA, Broccoli A and Stouffer RJ (2005) Assessing the role of North Atlantic freshwater forcing in millennial scale climate variability: a tropical Atlantic perspective. *Climate Dynamics* **24**, 325–46.

Dansgaard W (1964) Stable isotopes in precipitation. *Tellus* **16**, 436–68.

Deplazes G, Luckge A, Stuut J-BW, Patzold J, Kuhlmann H, Husson D, Fant M and Haug GH (2014) Weakening and strengthening of the Indian monsoon during Heinrich events and Dansgaard-Oeschger oscillations. *Paleoceanography* **29**, 99–144.

Dong JG, Shen C-C, Kong XG, Wang YJ and Duan FC (2018) Asian monsoon dynamics at Dansgaard/Oeschger events 14-8 and Heinrich events 5-4 in northern China. *Quaternary Geochronology* **47**, 72–80.

Dong XY, Kathayat G, Rasmussen SO, Svensson A, Severinghaus JP, Li HY, Sinha A, Xu Y, Zhang HW, Shi ZG, Cai YJ, Pérez-Mejías C, Baker J, Zhao JY, Spötl C, Columbu A, Ning YF, Stríkis NM, Chen ST, Wang XF, Gupta AK, Dutt S, Zhang F, Cruz FW, An ZS, Edwards RL and Cheng H (2022) Coupled atmosphere-ice-ocean dynamics during Heinrich Stadial 2. *Nature Communications* **13**, 5867.

Draxler RR and Hess GD (1998) An overview of the HYSPLIT_4 modelling system for trajectories, dispersion, and deposition. *Australian Meteorology magazine* **47**, 295–308.

Dutt S, Gupta AK, Clemens SC, Cheng H, Singh RK, Kathayat G and Edwards RL (2015) Abrupt changes in Indian summer monsoon strength during 33,800 to 5500 years B.P. *Geophysical Research Letters* **42**, 5526–32.

Dykoski C, Edwards RL, Cheng H, Yuan DX, Cai YJ, Zhang ML, Lin YS, Qing JM, An ZS and Revenaugh J (2005) A high-resolution, absolute-dated Holocene and deglacial Asian monsoon record from Dongge Cave, China. *Earth And Planetary Science Letters* **233**, 71–86.

Gong DY and Ho CH (2002) Shift in the summer rainfall over the Yangtze River valley in the late 1970s. *Geophysical Research Letters* **29**, 71–8.

Guo ZT, Liu T-S, Guiot J, Wu N, Lü HY and Han JM (1996) High frequency pulses of East Asia monsoon climate in the last two glaciations: link with the North Atlantic. *Climate Dynamics* **12**, 701–9.

Hiess J, Condon DJ, McLean N, Noble SR (2012) 238U/235U Systematics in terrestrial uranium– bearing minerals. *Science* **335**, 1610–1614.

Hu CY, Henderson GM, Huang JH, Xie SC, Sun Y and Johnson KR (2008) Quantification of Holocene Asian monsoon rainfall from spatially separated cave records. *Earth and Planetary Science Letters* **266**, 221–32.

Jacobel AW, McManus JF, Anderson RF and Winckler G (2016) Large deglacial shifts of the Pacific intertropical convergence zone. *Nature Communications* **7**, 10449.

Jaffey AH, Flynn KF, Glendenin LE, Bentley WC, Essling AM (1971) Precision measurement of half–lives and specific activities of 235U and 238U. *Physical Review C* **4**, 1889–1906.

Jiang DB, Lang XM, Tian ZP and Guo DL (2011) Last glacial maximum climate over China from PMIP simulations. *Palaeogeography Palaeoclimatology Palaeoecology* **309**, 347–57.

Kaboth-Bahr S, Bahr A, Yamoah KA, Chuang C-K, Li H-C, Su C-C and Wei K-Y (2021) Rapid humidity changes across the Northern South China Sea during the last ~40 kyrs. *Marine Geology* **440**, 106579.

Kucera M, Weinelt M, Kiefer T, Pflaumann U, Hayes A, Weinelt M, Chen M-T, Mix AC, Borrows TT, Cortijo E, Duprat J, Juggins S and Waelbroeck C (2005) Reconstruction of sea-surface temperatures from assemblages of planktonic foraminifera: multi-technique approach based on geographically constrained calibration data sets and its application to glacial Atlantic and Pacific Oceans. *Quaternary Science Reviews* **24**, 951–98.

Lachniet MS (2015) Are aragonite stalagmites reliable paleoclimate proxies? Tests for oxygen isotope time-series replication and equilibrium. *Geological Society of America Bulletin* **50**, 489–510.

Li D, Tan LC, Cai YJ, Jiang XY, Ma L, Cheng H, Edwards RL, Zhang HW, Gao YL and An ZS (2019) Is Chinese stalagmite $\delta^{18}O$ solely controlled by the Indian summer monsoon? *Climate Dynamics* **53**, 2969–83.

Li YX, Rao ZG, Cao JT, Jiang H and Gao YL (2017) Highly negative oxygen isotopes in precipitation in southwest China and their significance in paleoclimatic studies. *Quaternary International* **440**, 64–71.

Liang YJ, Zhao K, Edwards RL, Wang YJ, Shao QF, Zhang ZQ, Zhao B, Wang Q, Cheng H and Kong XG (2020) East Asian monsoon changes early in the last deglaciation and insights into the interpretation of oxygen isotope changes in the Chinese stalagmite record. *Quaternary Science Reviews* **250**, 106699.

Lisiecki LE and Stern JV (2016) Regional and global benthic $\delta^{18}O$ stacks for the last glacial cycle. *Paleoceanography* **31**, 1368–94.

Liu G, Li X, Chiang HW, Yuan S, Chawchai S, He S, Lu Y, Aung LT, Maung PM, Tun WN, Oo KM and Wang XF (2020) On the glacial-interglacial variability of the Asian monsoon in speleothem $\delta^{18}O$ records. *Science Advances* **6**, eaay8189, 1–10.

Liu JB, Chen JH, Zhang XJ, Li Y, Rao ZG and Chen FH (2015) Holocene East Asian summer monsoon records in northern China and their inconsistency with Chinese stalagmite $\delta^{18}O$ records. *Earth Science Reviews* **148**, 194–208.

Liu ZY, Wen XY, Brady EC, Otto-Bliesner B, Yu G, Lu HY, Cheng H, Wang YJ, Zheng WP, Ding YH, Edwards RL, Cheng J, Liu W and Yang H (2014) Chinese cave records and the East Asia summer monsoon. *Quaternary Science Reviews* **83**, 115–28.

Lynch-Stieglitz J, 2017. The Atlantic meridional overturning circulation and abrupt climate change. *Annual Review of Marine Science* **9**, 83–104.

Maher BA and Thompson R (2012) Oxygen isotopes from Chinese caves: records not of monsoon rainfall but of circulation regime. *Journal of Quaternary Science* **27**, 615–24.

Markle BR, Steig EJ, Buizert C, Schoenemann SW, Bitz CM, Fudge TJ, Pedro JB, Ding QH, Jones TR, White JWC and Sowers T (2016) Global atmospheric teleconnections during Dansgaard-Oeschger events. *Nature Geoscience* **10**, 36–40.

Mohtadi M, Prange M, Oppo DW, Pol-Holz RD, Merkel U, Zhang X, Steinke S and Luckge A (2014) North Atlantic forcing of tropical Indian Ocean climate. *Nature* **509**, 76–80.

Nagashima K, Tada R, Tani A, Sun Y, Isozaki Y, Toyoda S and Hasegawa H (2011) Millennial-scale oscillations of the westerly jet path during the last glacial period. *Journal of Asian Earth Sciences* **40**, 1214–20.

Pausata FSR, Battisti DS, Nisancioglu KH and Bitz CM (2011) Chinese stalagmite $\delta^{18}O$ controlled by changes in the Indian monsoon during a simulated Heinrich event. *Nature Geoscience* **4**, 474–80.

Porter S and An ZS (1995) Correlation between climate events in the North-Atlantic and China during the last glaciation. *Nature* **375**, 305–8.

Qiu H-Y, Li TY, Chen C-J, Huang R, Wang T, Wu Y, Xiao S-Y, Xu Y-Z, Huang Y-Y, Zhang J, Yang Y and Li JY (2021) Significance of active speleothem $\delta^{18}O$ at annual-decadal timescale: a case study from monitoring in Furong Cave. *Applied Geochemistry* **126**, 104873.

Qiu WY, Zhang X, Jiang XY, Hu HM, Ma L, Xiao HY, Cai BG and Shen C-C (2022) Double-plunge structure of the East Asian summer monsoon during Heinrich Stadial 1 recorded in Xianyun Cave, southeastern China. *Quaternary Science Reviews* **282**, 107442.

Sampe T and Xie SP (2010) Large-scale dynamics of the Meiyu-Baiu rainband: environmental forcing by the westerly jet. *Journal of Climate* **23**, 113–34.

Shen C-C, Wu C-C, Cheng H, Edwards RL, Hsieh Y-T, Gallet S, Chang C-C, Li T-Y, Lam DD, Kano A, Hori M and Spötl C (2012) High-precision and high-resolution carbonate ^{230}Th dating by MC-ICP-MS with SEM protocols. *Geochimica et Cosmochimica Acta* **99**, 71–86.

Siddall M, Rohling EJ, Almogl-Labin A, Hemleben Ch, Meischner D, Schmelzer I and Smeed DA (2003) Sea-level fluctuations during the last glacial cycle. *Nature* **432**, 853–8.

Siddall M, Rohling EJ, Thompson WG and Waelbroeck C (2008) Maine isotope stage 3 sea level fluctuations: data synthesis and new outlook. *Reviews of Geophysics* **46**, RG4003.

Sun YB, Chen J, Clemens SC, Liu QS, Ji JF and Tada R (2006) East Asian monsoon variability over the last seven glacial cycles recorded by a loess sequence from the northwestern Chinese Loess Plateau. *Geochemistry Geophysics and Geosystems* **7**, 1–16.

Sun YB, Clemens SC, Morrill C, Lin XP, Wang XL and An ZS (2012). Influence of Atlantic meridional overturning circulation on the East Asian winter monsoon. *Nature Geoscience* **5**, 46–9.

Tan M (2009) Circulation effect: climatic significance of the short term variability of the oxygen isotopes stalagmites form monsoonal China—dialogue between paleoclimate records and modern climate research. *Quaternary Science* **29**, 851–62 (in Chinese with English abstract).

Tan M (2011) Trade-wind driven inverse coupling between stalagmite δ18O from monsoon region of China and large scale temperature. *Quaternary Science* **31**, 1086–97 (in Chinese with English abstract).

Tan M (2013) Circulation effect: response of precipitation $\delta^{18}O$ to the ENSO cycle in monsoon regions of China. *Climate Dynamics* **42**, 1067–77.

Tan M (2016) Circulation background of climate patterns in the past millennium: uncertainty analysis and re-reconstruction of ENSO-like state. *Science China Earth Science* **59**, 1225–41.

Tierney JE, Pausata FSR and DeMenocal P (2016) Deglacial Indian monsoon failure and North Atlantic Stadials linked by Indian Ocean surface cooling. *Nature Geoscience* **9**, 46–50.

Wang HJ and Chen HP (2012) Climate control for southeastern China moisture and precipitation: Indian or East Asian monsoon? *Journal of Geophysical Research: Atmospheres* **117**, 1–9.

Wang YJ, Cheng H, Edwards RL, An ZS, Wu JY, Shen C-C and Dorale JA (2001) A high-resolution absolute-dated Late Pleistocene monsoon record from Hulu Cave, China. *Science* **294**, 2345–8.

Yang XL, Liu JB, Liang FY, Yuan DX, Yang Y, Lu YB and Chen FH (2014) Holocene stalagmite $\delta^{18}O$ records in the East Asian monsoon region and their correlation with those in the Indian monsoon region. *Holocene* **24**, 1657–64.

Yuan DX, Cheng H, Edwards RL, Dykoski CA, Kelly MJ, Zhang ML, Qing JM, Lin YS, Wang YJ, Wu JY, Dorale JA, An ZS and Cai YJ (2004) Timing, duration, and transitions of the last interglacial Asian monsoon. *Science* **304**, 575–8.

Zhang HW, Cai YJ, Tan LC, Qin SJ and An ZS (2014) Stable isotope composition alteration produced by the aragonite-to-calcite transformation in speleothems and implications for paleoclimate reconstructions. *Sedimentary Geology* **309**, 1–14.

Zhang R and Delworth TL (2005) Simulated tropical response to a substantial weakening of the Atlantic thermohaline circulation. *Journal of Climate* **18**, 1853–60.

Zhang X, Qiu WY, Jiang XY, Hu HM, Xiao HY, Cai BG and Shen C-C (2021) Three-phase structure of the East Asia summer monsoon during Heinrich

https://doi.org/10.1017/S0016756824000013

Stadial 4 recorded in Xianyun Cave, southeastern China. *Quaternary Science Reviews* **274**, 107267.

Zhao JY, Cheng H, Yang Y, Tan LC, Spötl C, Ning YF, Zhang HW, Cheng X, Sun Z, Li XL, Li HY, Liu W and Edwards RL (2019) Reconstructing the Western boundary variability of the Western Pacific subtropical high over the past 200 years via Chinese cave oxygen isotope records. *Climate Dynamics* **52**, 3741–57.

Zhao SH, Liu ZF, Colin C, Zhao YL, Wang XX and Jian ZM (2018) Responses of the East Asian summer monsoon in the low-latitude South China Sea to high-latitude millennial-scale climatic changes during the last glaciation: evidence from a high-resolution clay mineralogical record. *Paleoceanography and Paleoclimatology* **33**, 2017PA003235.

Zhou HY, Zhao JX, Feng YX, Gagan MK, Zhou GQ and Yan J (2008) Distinct climate change synchronous with Heinrich event one, recorded by stable oxygen and carbon isotopic compositions in stalagmites from China. *Quaternary Research* **69**, 306–15.

Zhou TJ, Yu R, Zhang J, Drange H, Cassou C, Deser C, Hodson DLR, Sanchez-Gomez E, Li J, Keenlyside N, Xin XG and Okumura Y (2009) Why the Western Pacific subtropical high has extended westward since the late 1970s. *Journal of Climate* **22**, 2199–215.

Zorzi C, Goñi MFS, Anupama K, Prasad S, Hanquiez V, Johnson J and Giosan L (2015) Indian monsoon variations during three contrasting climatic periods: the Holocene, Heinrich Stadial 2, and the last interglacial-glacial transition. *Quaternary Science Reviews* **125**, 50–60.

https://doi.org/10.1017/S0016756824000013